Journal of Marine Science and Technology

Volume 28 | Issue 4 Article 9

BOREHOLE BREAKOUT ANALYSIS AND PHYSICAL PROPERTIES OF COSTA RICA CONVERGENT MARGIN SEDIMENTS: INTEGRATED OCEAN DRILLING PROGRAM (IODP) EXPEDITION 334

Gil Young Kim
Petroleum & Marine Division, Korea Institute of Geoscience and Mineral Resources (KIGAM), 124 Gwahak-ro, Yuseong-gu, Daejeon 305-350, South Korea, gykim@kigam.re.kr

Buyanbat Narantsetseg
Department of Petroleum and Drilling, Mongolian Science and Technology University, 216046 Ulaanbaatar, Mongolia

Recommended Citation

Kim, Gil Young and Narantsetseg, Buyanbat (2020) "BOREHOLE BREAKOUT ANALYSIS AND PHYSICAL PROPERTIES OF COSTA RICA CONVERGENT MARGIN SEDIMENTS: INTEGRATED OCEAN DRILLING PROGRAM (IODP) EXPEDITION 334," *Journal of Marine Science and Technology*: Vol. 28: Iss. 4, Article 9.
DOI: 10.6119/JMST.202008_28(4).0009
Available at: https://jmstt.ntou.edu.tw/journal/vol28/iss4/9

BOREHOLE BREAKOUT ANALYSIS AND PHYSICAL PROPERTIES OF COSTA RICA CONVERGENT MARGIN SEDIMENTS: INTEGRATED OCEAN DRILLING PROGRAM (IODP) EXPEDITION 334

Acknowledgements

The data used herein were provided by the IODP. We thank the support provided by the JOIDES Resolution drilling crew, logging staff, laboratory technicians, and the physical property team. This research was a part of the project titled “International Ocean Discovery Program” funded by Ministry of Oceans and Fisheries, Korea. This research was also funded by Korea Institute of Geoscience and Mineral Resources (KIGAM 20-3312-1).

Journal of Marine Science and Technology, Vol. 28, No. 4, pp. 311-320 (2020)
DOI: 10.6119/JMST.202008_28(4).0009

BOREHOLE BREAKOUT ANALYSIS AND PHYSICAL PROPERTIES OF COSTA RICA CONVERGENT MARGIN SEDIMENTS: INTEGRATED OCEAN DRILLING PROGRAM (IODP) EXPEDITION 334

Gil Young Kim[1] and Buyanbat Narantsetseg[2]

Key words: IODP 334, borehole image, in situ stress, physical property, convergent margin.

ABSTRACT

Borehole image and physical properties data from two sites (U1378, U1379) drilled during the Integrated Ocean Drilling Program (IODP) Expedition 334 were analyzed to study the effect of erosional subduction at the Costa Rica convergent margin. The various laboratory and log data were collected from Logging-While-Drilling (LWD), moisture and density analysis (MAD), and Multisensor Core Logger tools (MSCL). Borehole breakouts interpreted from image data acquired from LWD were identified and analyzed using GMI Imager software. In this study, borehole breakouts from holes U1378A and U1379A showed different borehole shape and stress directions, indicating different present-day *in situ* stress orientation at the two sites. In U1378A, the azimuths of breakouts are from 52.21 to 58.14 degrees, and the widths of breakout are variable (52.46–70.55 degree) with depth. Conversely, the azimuths of breakouts in U1379A are from 106.79 to 116.53 degrees and the widths are variable (51.43–57.89 degrees) with depth. This suggests that present-day upper plate movement in these two sites may be in different directions, related to transition between a compressional regime and extension and subsidence. Generally, the physical properties measured from core samples were in agreement with the log data, and reflected well both lithology and burial effect.

Paper submitted 10/31/19; revised 03/24/20; accepted 04/27/20. Corresponding Author: Gil Young Kim(E-Mail gykim@kigam.re.kr)
[1] Petroleum & Marine Division, Korea Institute of Geoscience and Mineral Resources (KIGAM), 124 Gwahak-ro, Yuseong-gu, Daejeon 305-350, South Korea
[2] Department of Petroleum and Drilling, Mongolian Science and Technology University, 216046 Ulaanbaatar, Mongolia

I. INTRODUCTION

The Costa Rica convergent margin is considered an ideal region to investigate the balance of sediment accretion, sediment subduction, and subduction erosion at the leading edge of a convergent margin, because of the rapid subduction rate (von Huene et al., 1995; Kimura et al., 1997). Generally, subducting plates transport a large volume of crustal materials and accompanying pore fluids to convergent margins. The physical and mechanical properties of subducted materials and fluids control the architecture, mass balance, and seismogenic behavior of actively convergent margins (Bangs and Westbrook, 1991; von Huene and Scholl, 1991; Moore and Vrolijk, 1992; Bangs et al., 1999; Bilek and Lay, 1999; Husen and Kissling, 2001; Moore and Saffer, 2001; Gettemy and Tobin, 2003).

The objective of the Integrated Ocean Drilling Program (IODP) Expedition 334 was to understand the processes that control nucleation and seismic rupture of large earthquakes at erosional subduction zones such as the Costa Rica margin (Vannucchi et al., 2012). During IODP Expedition 334, four sites were drilled at the Costa Rica margin (Table 1). The northwestern area of Expedition 334 had previously been drilled during Deep Sea Drilling Project (DSDP) Leg 84 and Ocean Drilling Program (ODP) Legs 170 and 205 (Fig. 1). Logging-while-drilling (LWD) was used during IODP Expedition 334 to measure the physical properties of the convergent margin area sediments. During drilling of the boreholes to be discussed here, Schlumberger LWD tools including the geoVISION 675 (near-bit electrical resistivity, resistivity images, and natural gamma radiation (NGR)), the arcVISION 675 (annular borehole pressure, resistivity, and NGR), the adnVISION 675 (neutron porosity and azimuthal measurements of ultrasonic caliper and bulk density), and the MWD Telescope 675 (drilling mechanics data and real-time telemetry) were located just above the drill bit.

Borehole breakouts, consisting of spalling along the borehole wall in stress-related preferential directions, have been

Table 1. General summary of IODP Exp. 334 site. Hole A is for LWD/Drilling. Holes B/C are for coring. LWD: Logging While Drilling, mbrf: meter below rig floor.

Site / Hole	Location		Seafloor depth (mbrf)	Phase	Total penetration (m)
	Latitude	Longitude			
U1378A	08°35.5415'N	084°04.6313'W	536.6	LWD	456.9
U1378B	08°35.5408'N	084°04.6315'W	533.2	Coring	523.9
U1379A	08°40.8501'N	084°02.0166'W	137.0	LWD	962.8
U1379B	08°40.8502'N	084°02.0277'W	138.5	Coring	10.5
U1379C	08°40.8605'N	084°02.0274'W	138.8	Coring	949.0
U1380A	08°35.9976'N	084°04.4032'W	515.0	Coring/ Drilling	482.4
U1381A	08°25.7150'N	084°09.4690'W	2080.2	Coring	164.1
U1381B	08°25.7149'N	084°09.4805'W	2080.2	Coring/Drilling	90.0

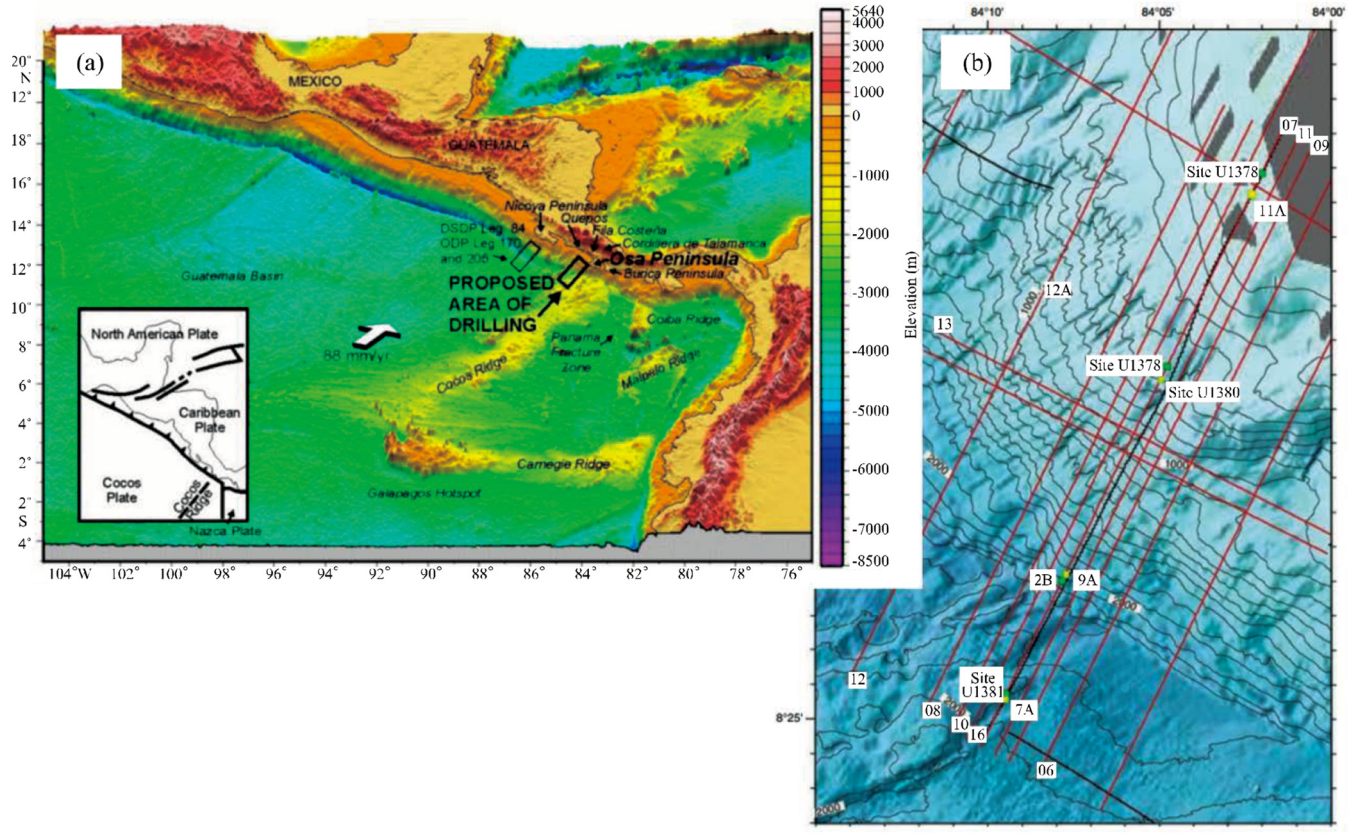

Fig. 1. Topographic and bathymetric map of the Costa Rica area including IODP Exp. 334 drilling area (a), showing location of Expedition 334 drilling sites (b). Note the collision of Cocos Ridge with the trench offshore the Osa Peninsula. DSDP = Deep Sea Drilling Project, ODP = Ocean Drilling Program (from Vannucchi et al., 2012).

used extensively for the interpretation of stress orientation and magnitude (Zoback, 2007). Recently, borehole image analysis of breakouts was applied to poorly consolidated sediments and the breakout-derived stress direction and magnitude were shown to closely match empirical measurements (Moore et al., 2009; Tobin et al., 2009; Chang et al., 2010), similar to breakouts investigated in hard rocks. Based on the borehole breakout analysis obtained from IODP Expedition 334, Malinverno et al. (2016) has been reported horizontal principal orientation in the Costa Rica Seismogenesis Project (CRISP) area. However, they didn't consider their characteristics according to depth intervals as well as interpretation related to physical property.

In this study, we analyzed borehole breakouts (e.g., shape,

width, diameter, frequency, and azimuth) from LWD image data, derived stress direction and magnitude, and then compared breakout data with other physical property data to investigate the relationship between the two data types. In addition to image analysis, whole-round multisensor core logger (MSCL) and natural gamma radiation logger (NGRL) tools were used to measure gamma ray density, magnetic susceptibility, compressional wave velocity, and natural gamma. Physical properties (water content, porosity, bulk density, grain density) for discrete core samples were measured by the weight-volume method.

Here, we first present the direction of stress in the borehole from borehole image analysis of factors such as shape, width, and frequency of breakouts with increasing borehole depth. Second, we interpret physical properties for convergent margin sediments. Finally, based on the results from these analyses, we try to interpret the relationship between borehole breakout and sediment characteristics such as lithology and hydration.

II. COSTA RICA CONVERGENT MARGIN

The oceanic Cocos plate subducting beneath Costa Rica has been formed by both the East Pacific Rise (EPR) and the Cocos-Nazca Spreading Center (CNS), and has been significantly influenced by Galapagos hotspot volcanism. The largest geographic feature formed by the passage of the Cocos plate over the Galapagos hotspot is the 2.5 km high Cocos Ridge. The oceanic crust beneath the Cocos Ridge is three times thicker than normal oceanic crust (Stavenhagen et al., 1998). A large number of seamounts formed by interaction with the Galapagos hotspot lie on the Cocos plate, resulting in a rather rough plate morphology including linear ridges and plateaus (Hey, 1977).

Off the northern Pacific coast of Costa Rica, the Cocos plate internal structure is dominated by large-offset, curved normal faults developed in response to downward bending of the subducting plate (Ranero et al., 2003, 2005). Southward along the Pacific coast, the plate structure transitions to a poorly developed trench with fewer normal faults. Where the Cocos Ridge subducts off the Osa Peninsula near the southernmost Pacific coast of Costa Rica, undisturbed sediments overlie normal faults and faulted blocks that must be older and unrelated to subduction (Ranero et al., 2005). From the northern Pacific coast of Costa Rica near the south end of the Nicoya Peninsula, crustal thickness increases southward to a maximum of 10-12 km related to thickening at the Cocos Ridge (Walther, 2003); age decreases along this same trend, and the relative buoyancy of the younger crust results in a relatively shallow dip of the subducting plate (Harris et al., 2010).

The Cocos plate at the Costa Rica convergent margin is being subducted beneath the Caribbean plate, with a rate of convergence of approximately 8–9 cm/yr (Demets et al., 1990) and in a direction almost perpendicular to the Middle America Trench. Claystones and silty claystones of Pliocene-Pleistocene age comprise the uppermost sediments on the subducting plate, and these are underlain by siliceous nannofossil chalk and calcareous diatomites (Vannucchi et al., 2012).

At IODP Expedition 334 sites, the middle slope site (Site U1378) used for this study is compressional area, whereas that at the upper slope site (Site U1379) is extensional area (Vannucchi et al., 2012). Thus, the marked change in stress state can be occurred along the CRISP transect in the northwestern flank of the Cocos Ridge and may correspond to a change from compression to extension, marking the onset of subduction erosion between Sites U1378 and U1379 (Malinverno et al., 2016).

III. METHODS

3.1 Analysis of Borehole Breakout from LWD Image Data

Schlumberger near-bit LWD tools collected continuous borehole density and ultrasonic measurements to produce images of electrical resistivity, bulk density, and borehole radius. Generally the resistivity images have the highest spatial resolution, but we used borehole radius and density data due to poor resolution of resistivity data. Breakouts in the hole U1378A were investigated in the unwrapped LWD images throughout the hole and mainly found in depth intervals between 110 and 438 meters below seafloor (mbsf). Breakouts in the hole U1379A were identified from 166 to 890 mbsf. Breakouts form in the minimum stress direction, and drilling-induced tensile fractures are formed in the maximum stress direction. GMI imager software (GeoMechanics International, Inc.) was used to analyze breakouts for each borehole.

3.2 Physical Property Data

Physical properties were measured for whole-round core, split core, and discrete core samples in both sites U1378 (holes U1378C and U1379C for coring). Gamma ray density, magnetic susceptibility, and compressional wave velocity were measured for whole-round core using multisensory core logger (MSCL) installed on the *JOIDES Resolution* research vessel. In addition, natural gamma for whole-round core was measured using the Natural Gamma Radiation Logger (NGRL) on the *JOIDES Resolution*. For moisture and density (MAD) measurement for discrete samples, cubic samples were cut from the working halves of split cores at an interval of 1 sample per section. The MAD water content, porosity, bulk density, and dry density was measured by the weight-volume method (Boyce, 1976). The MAD facility on the *JOIDES Resolution* includes a dual-balance system (Mettler-Toledo XS204) and a hexapycnometer (refer method chapter in the proceedings of IODP Expedition 334 for detailed explanation). Grain size analysis from MAD samples was also determined using a Sedigraph 5100 (Micromeritics) at Korea Institute of Geoscience and Mineral Resources (KIGAM). Textural parameters and relative amounts of sand, silt, and clay were calculated using the classifications of Folk and Ward (1957) and Folk (1968).

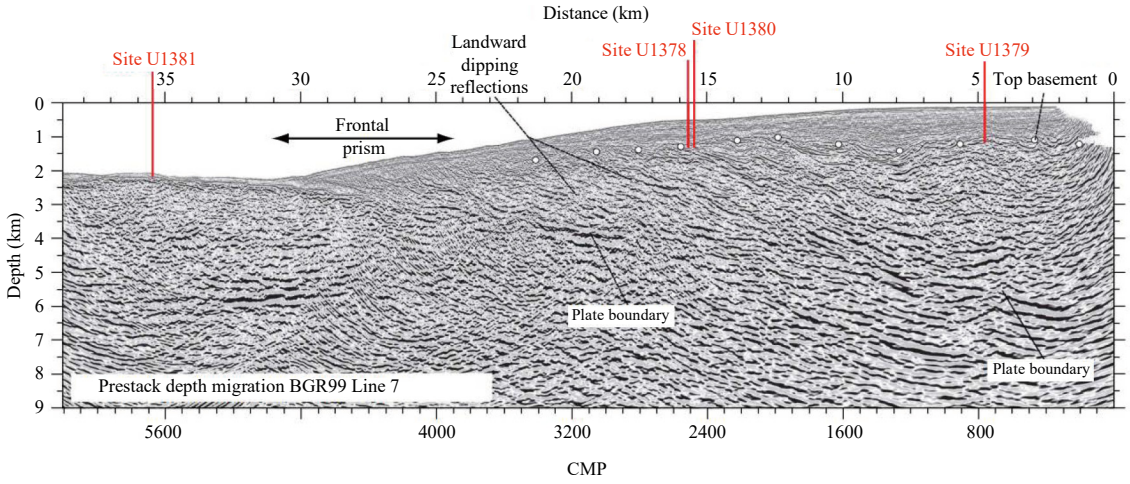

Fig. 2. Seismic BGR99 Line 7 showing location of four drill sites across Costa Rica margin offshore Osa Peninsula. Prestack depth migration (C.R. Ranero, unpublished data) is at a vertical exaggeration of 1.3×. CMP = common midpoint.

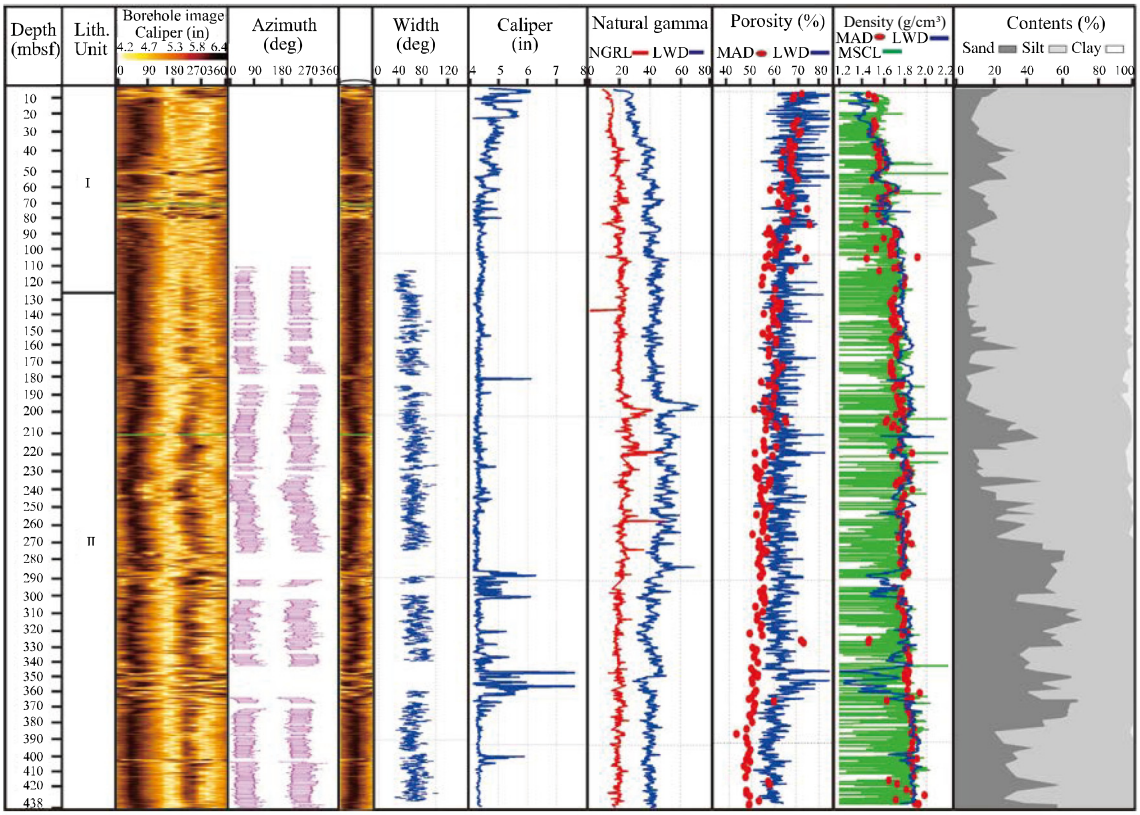

Fig. 3. Results of breakouts analysis and physical property measurements at Site U1378. The azimuth and width of borehole breakouts are displayed. The physical properties measured from LWD log, MAD, and whole-round core are also presented. NGRL= natural gamma radiation logger, MAD= moisture and density, MSCL= multisensor core logger. The contents of sand, silt, and clay are displayed.

IV. RESULTS AND DISCUSSION

4.1. Physical Property Variation

4.1.1. Site U1378 (hole U1378B)

Site U1378 is located in an area of the middle slope with a relatively thick sequence of slope sediment (Fig. 2). The margin consists of approximately 750 m of slope sediments overlying upper plate basement (Vannucchi et al., 2012). Site U1378 was drilled to investigate the nature and deformation of

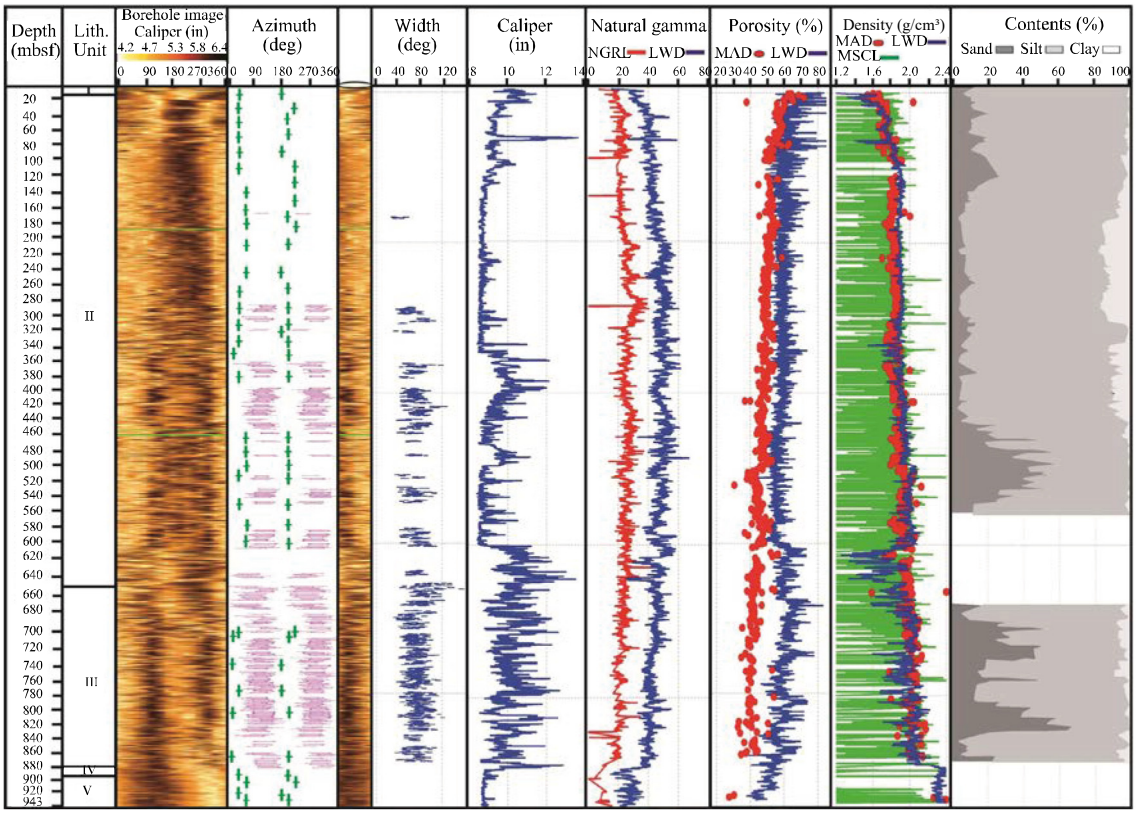

Fig. 4. Results of breakouts analysis and physical property measurements at Site U1379. The azimuth and width of borehole breakouts are displayed. The physical properties measured from LWD log, MAD, and whole-round core are also presented. NGRL= natural gamma radiation logger, MAD= moisture and density, MSCL= multisensor core logger. The contents of sand, silt, and clay are displayed.

the midslope sedimentary sequence and the uppermost portions of the basement imaged by multi-channel seismic data.

Site U1378 can be divided into two lithostratigraphic units (Vannucchi et al., 2012). Unit I is from seafloor to 127.83 mbsf, consisting of dark greenish gray and soft silty clay sediments. The main composition of Unit I is terrigenous minerals with silt dominant. Unit II is from 127.83 to 513.56 mbsf (Fig. 3). This unit consists of olive-green clayey silt (stone) and silty clay (stone) with minor layers of sand (stone), and tephra. The sediments of Unit II are firm and well consolidated with massive formation. The detailed description of lithology at Site U1378 was previously reported in the proceedings of the IODP (Vannucchi et al., 2012).

As shown in Fig. 3, physical properties of Site U1378 show a general pattern changing from 70 to 50% in porosity, and from 1.3 to 2.0 g/cm^3 in density, with burial depth. Natural gamma shows a significant excursion around 200 mbsf, indicating an increase in clay content compared with other intervals; in addition, scoria occurring in this interval could be responsible for the high natural gamma (Vannucchi et al., 2012).

Caliper data above 25 mbsf indicate borehole collapse during drilling, presumably because of soft upper sediments, caused by fast drilling penetration (Vannucchi et al., 2012). In addition, the intervals between 285 and 300 mbsf, and between 350 and 365 mbsf are also out-of-gauge, characterized by large caliper values (greater than 5 inches in radius; Fig. 3), which adversely affects LWD, especially density. Below 275 mbsf, there are the out-of-gauge intervals, caused by high sand content compared to other intervals (Fig. 3). The densities measured by other methods show a similar pattern in the most intervals. On the other hand, porosity variation with burial depth is characterized by increasing deviation (approximately 10%) between LWD and MAD (Fig. 3), coinciding well with increasing sand content (~60%). Generally, the neutron porosity measured from LWD can be overestimated in clay-rich sediments because of hydrogen in clay mineral (Ellis, 1986). However, this data is opposite pattern. Overall, physical properties are mainly affected by lithology and by compaction associated with burial depth, as reported by the previous studies (Hamilton, 1980; Hamilton and Bachman, 1982). Therefore, further research is needed.

4.1.2. Site U1379 (hole 1379C)

Site U1379 (Fig. 2) is located in an area of the upper slope, with 890 m of slope sediment overlying the upper plate basement (Vannucchi et al., 2012). Site U1379 was drilled to identify the lithostratigraphy of the upper slope sequence and the uppermost portions of the basement investigated by seismic data. Site U1379 cores are divided into five lithostratigraphic units (Fig. 4). Unit I encompasses from seafloor to 0.93 mbsf,

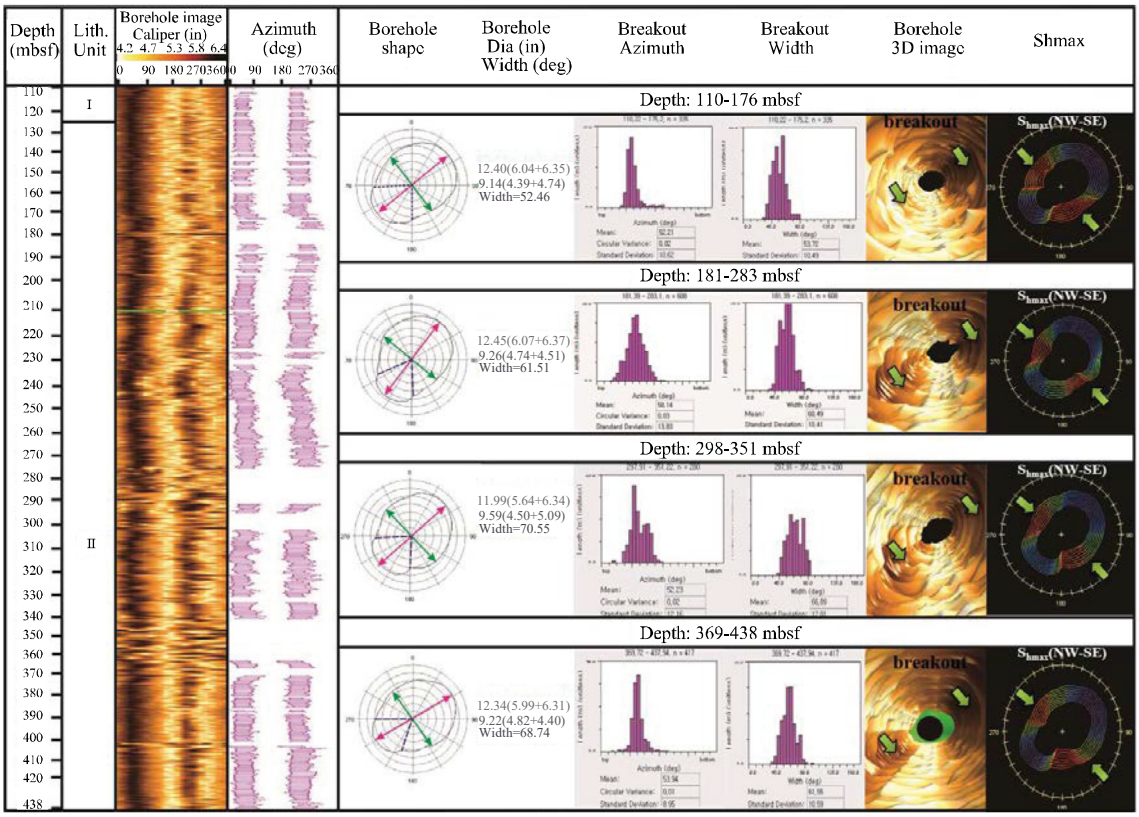

Fig. 5. Analysis of borehole breakouts from borehole image data collected from the hole U1378A. The borehole breakouts are identified in four depth intervals (110-176 mbsf, 181-283 mbsf, 298-351 mbsf, and 369-438 mbsf). Note the maximum horizontal stress direction of NW-SE. Shmax= maximum horizontal stress.

consisting of a medium- to coarse-grained sand with shell fragments. Unit II, from 0.93 to 651 mbsf, consists of olive-green clayey silt (stone) and silty clay (stone) with minor layers of sand (stone), and tephra; the sediment is firm and well consolidated. Unit III, from 651 to 880.07 mbsf, consists of olive-green silty sands and sandstone. Unit IV, from 879.90 to 881.75 mbsf, is composed of carbonate-cemented medium- to coarse-grained sand with well-rounded, lithic pebble-sized clasts and thick-wall shell shards. Unit V, from 881.75 to 947.52 mbsf, consists of matrix-supported breccia with clasts of limestone, basalt, and mudstone. The detailed description of lithology at Site U1379 was previously reported in the proceedings of the IODP (Vannucchi et al., 2012).

As shown in Fig. 4, physical properties of Site U1379 show a general pattern, changing from 70 to 40% in porosity, and from 1.4 to 2.1 g/cm^3 in density, with burial depth. Natural gamma likely reflects clay content. Caliper data above 20 mbsf indicates borehole collapse during drilling of soft upper sediments. In addition, the intervals between 350 and 450 mbsf, and between 620 and 880 mbsf are characterized by large caliper values (greater than 11 inches in diameter; Fig. 4) and showing LWD low density. In these intervals, sand contents are relatively higher than in other intervals (Fig. 4). Below 620 mbsf, difference of porosity from LWD and MAD increases significantly (>10%) compared with that in the upper sections, likely related to increasing sand content (>40%). The densities from LWD and MAD throughout this hole are relatively consistent, except for the interval of out-gauge hole showing low density on LWD data.

4.2. Characteristics of Borehole Breakouts

4.2.1. Site U1378 (hole U1378A)

At Site U1378 (middle continental slope), there are no observable breakouts in the upper part of hole. However, below 110 mbsf, breakouts appear as two vertical dark bands in both density and radius images (Fig. 3, and Fig. 5). We identified separate breakouts for the intervals 110–176 mbsf, 181–283 mbsf, 298–351 mbsf, and 369–438 mbsf (Fig. 5). In particular, the borehole radius images were used to identify the breakout morphology throughout the hole (Fig. 5).

As shown in Fig. 3 and Fig. 5, breakouts occur continuously as two well-developed vertical bands (both borehole image and azimuth degree) of large borehole radius separated by 180° in the lower part of hole. As shown in Figure 5, deformation of borehole shape caused by borehole breakout was well identified. The diameter and width of borehole breakout were roughly calculated. The differences between long and short diameters of borehole show 2.4 (6.1 cm), 3.26 inches (8.2 cm),

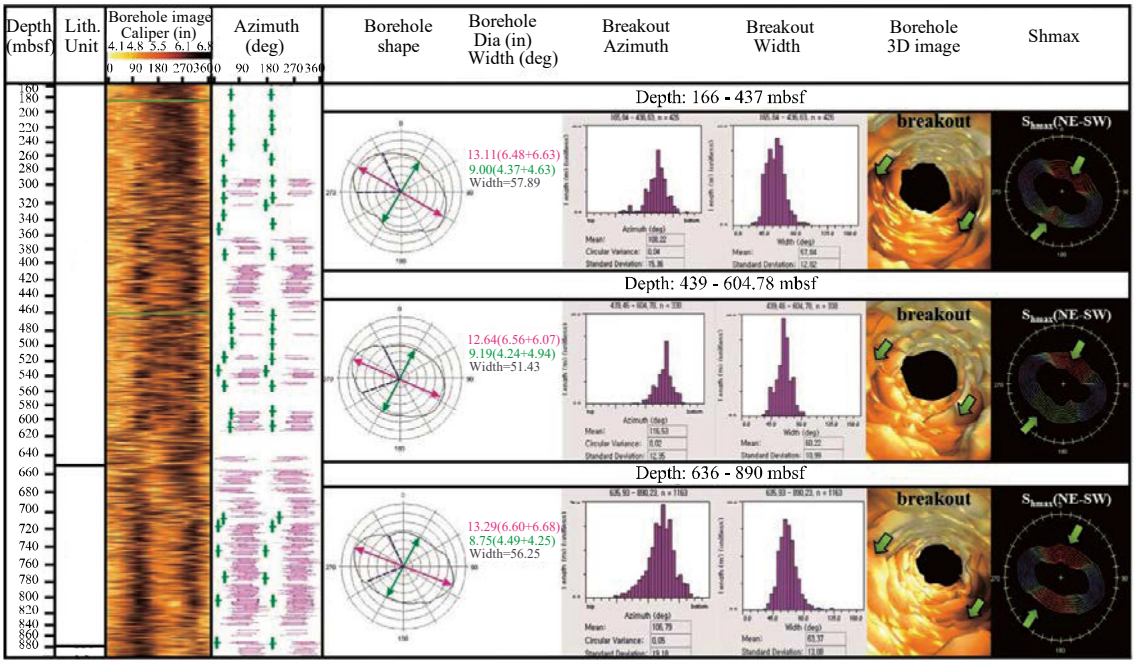

Fig. 6. Analysis of borehole breakouts from borehole image data collected from the hole U1379A. The borehole breakouts are identified in three depth intervals (166-437, 439-604, and 636-890 mbsf). Note the maximum horizontal stress direction of NE-SW. Shmax= maximum horizontal stress.

and 2.95 inches (7.5 cm) on average compared with diameter of in-gauge hole. The azimuths of breakouts are from 52.21 to 58.14 degrees. The widths of breakout are variable (52.46–70.55 degrees) with depth. Shape of each breakout is identified in the 3D image of borehole.

From breakout shape, we roughly estimated the maximum horizontal stress direction. Generally, the borehole breakouts also provide useful information on stress magnitudes (Gough and Bell, 1982). The principle is that the width of the breakout is dependent on the stress magnitudes and the compressive strength of the borehole wall rock. However, to estimate the range of stress magnitudes, further study is needed in the future. Overall, breakouts in U1378 are developed in a northeast-southwest orientation, indicating that the maximum horizontal stress (green arrows in Fig. 5) may be oriented northwest to southeast. This stress direction was anticipated, given geological structure (e.g., fold and fault direction) in a previously investigated core sample (Vannucchi et al., 2012) and fracture analysis of LWD data (Saito et al., 2011; Malinverno et al., 2016). Generally, breakouts have been known as tending to increase with increasing clay content (Trautwein-Bruns et al., 2010). However, there is no relation due to the very low content of clay content at Site U1378 (Fig. 3).

4.2.2. Site U1379 (hole 1379A)

At Site U1379 (upper continental slope), no breakouts were observed above 160 mbsf. Breakouts displayed as two vertical dark bands in both density and radius images (Fig. 4 and Fig. 6) in the intervals 166–437 mbsf, 439–604 mbsf, and 636–890 mbsf (Fig. 6). Similar to Site U1378, the borehole radius images were used to identify the breakout morphology throughout the hole (Fig. 6).

As shown in Fig. 4 and Fig 6, breakouts occur continuously as two parallel, vertical bands (both borehole image and azimuth degree) of large borehole radius, 180° apart, where they occur between the depths of 160 and 880 mbsf. As shown in Fig. 6, deformed borehole shape caused by breakout was clearly identifiable. The differences between long and short diameters of borehole are 3.45 (8.8 cm), 4.54 inches (11.5 cm), and 4.03 inches (10.2 cm) on average compared with the diameter of in-gauge hole. The azimuths of breakouts are from 106.79 to 116.53 degrees, notably different from Site U1378. The widths of breakout in U1379 are variable (51.43–57.89 degrees) with depth.

Shapes of breakouts in U1379 are shown in the 3D image of the borehole. Overall, breakouts are developed in a northwest-southeast orientation, indicating that the maximum horizontal stress (green arrows in Fig. 6) may be oriented northeast to southwest. This stress direction was previously noted from geological structure (e.g., fold and fault direction) investigated in U1379 core samples (Vannucchi et al., 2012), and in fracture analysis based on LWD data (Saito et al., 2011; Malinverno et al., 2016). Occurrence of breakouts with burial depth seems to be related more to sand occurrence in this case than to the clay content dependency suggested by Trautwein-Bruns et al. (2010); therefore, the relationship between clay content and breakout may not be clear yet.

Tensile fractures are identified at three depth intervals in U1379, including 1–260 mbsf, 260–620 mbsf, and 700–943 mbsf (Fig. 7). Tensile fractures induced in the wellbore wall

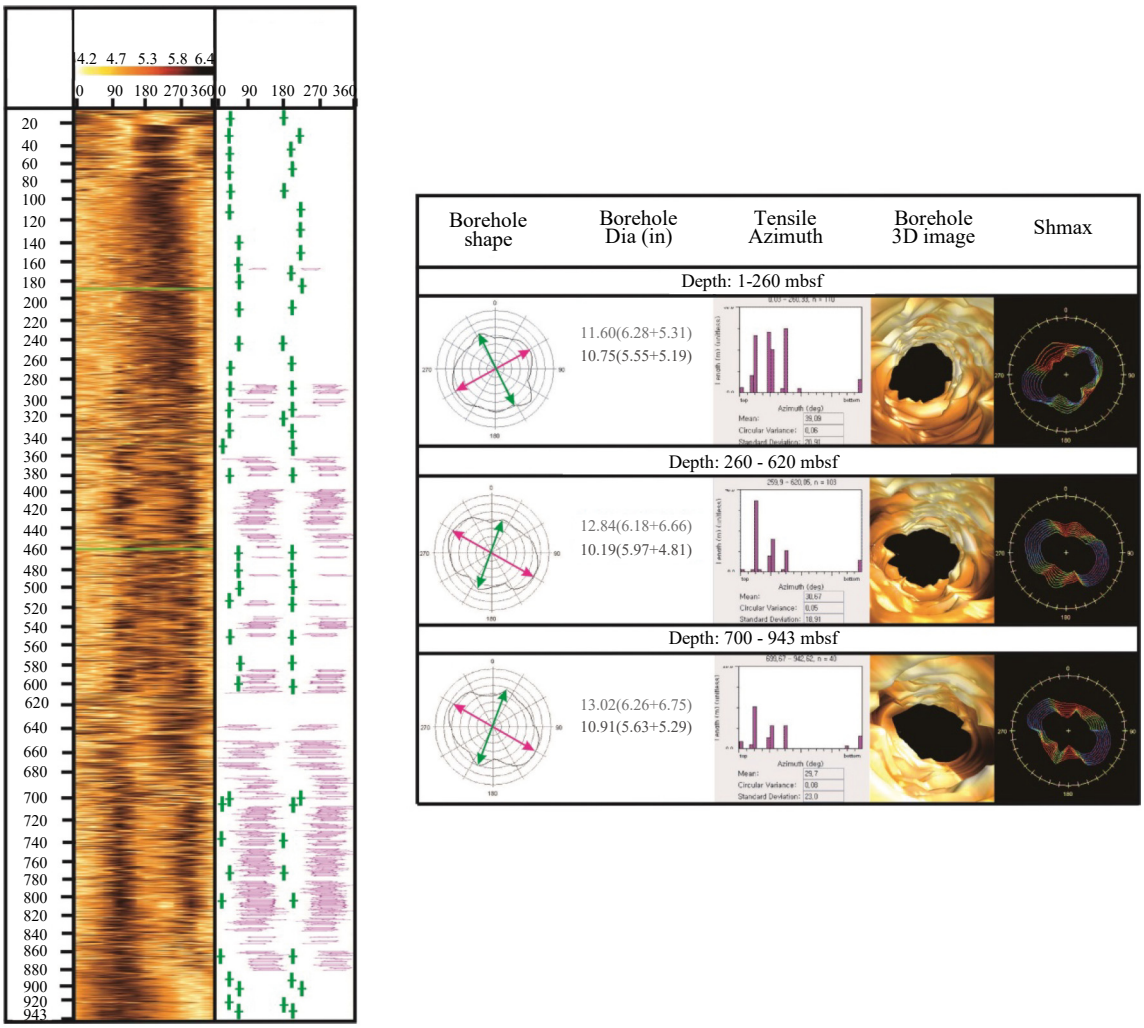

Fig. 7. Analysis of tensile fractures from borehole image data collected from the hole U1379A. The tensile fractures are identified in three depth intervals (1-260, 260-620, and 700-943 mbsf). Note the tensile fracture occurring along the perpendicular to borehole breakouts.

during drilling generally occur perpendicular to borehole breakout. Thus tensile fracture orientation can be a reliable indicator of the orientation of the maximum horizontal principal stress (Brudy and Zobak, 1998). In this study, tensile fractures are rarely seen which are inclined to the wellbore axis (Fig. 7). However, the origin of tensile fractures in U1379 is not clear, and it is unknown whether they were created during the drilling process or were preexisting features (e.g., natural fractures) crosscut by the wall. Based on the investigation of core samples, there are many fractured and brecciated zones, caused by normal fault (Vannucchi et al, 2012). Thus, these zones can be the cause of tensile fractures. For a detailed explanation of drilling-induced fractures, further investigation of rock mechanics is needed, beyond the scope of this study. As shown in Fig. 7, the azimuths of tensile fractures are from 29.7–39.9 degrees.

In summary, the maximum principal horizontal stress is directed NE-SW at Site U1378 and NW-SE at Site U1379. This result supported well by the previous result (Malinverno et al., 2016). Malinverno et al. (2016) suggested that the maximum principal horizontal stress directions may be influenced by the movement of Cocos Ridge and by the transition between aseismic and seismic subduction along the plate boundary. Thus the maximum stress direction of geologically complicated area would be very different. Nevertheless, the maximum horizontal stress pattern corresponds closely to plate motion around the study area, reflecting the orientation of the present-day maximum horizontal stress within the borehole, and in accordance with the regional stress field in this area (Vannucchi et al, 2012, 2013, 2014; Malinverno et al., 2016)..

V. CONCLUSIONS

Based on borehole breakout analysis, the breakout orientation at U1378A in the middle slope site indicates that the maximum horizontal stress is oriented northwest–southeast. On the other hand, at U1379A in the upper slope site, the maximum horizontal stress is oriented northeast-southwest. These

directions are probably related to complicated tectonic regimes (including compressional, transpressional, and extensional stress states) currently active in this area. The diameters of the boreholes generally show small variation with depth; however, the widths of breakouts are characterized by recognizable variation with depth, probably due to the difference of lithology of the borehole wall. Physical properties of the samples reflect both lithology and burial effect as expected. However, further study is needed for detailed interpretation related to direction and strength of plate movement in this area.

ACKNOWLEDGMENTS

The data used herein were provided by the IODP. We thank the support provided by the *JOIDES Resolution* drilling crew, logging staff, laboratory technicians, and the physical property team. This research was a part of the project titled "International Ocean Discovery Program" funded by Ministry of Oceans and Fisheries, Korea.

This research was also funded by Korea Institute of Geoscience and Mineral Resources (KIGAM 20-3312-1).

REFERENCES

Bangs, N.L.B. and G.K. Westbrook (1991). Seismic modeling of the decollement zone at the base of Barbados Ridge accretionary complex. Journal of Geophysical Research 96, 3852–3866.

Bangs, N.L.B., T.H. Shipley, J.C. Moore and G.F. Moore (1999). Fluid accumulation and channeling along the northern Barbados Ridge decollement thrust. Journal of Geophysical Research 104, 20399–20414.

Bilek, S.L. and T. Lay (1999). Rigidity variations with depth along interpolate megathrust faults in subduction zones. Nature 400, 443–446.

Boyce, R.E. (1976). Definition and laboratory techniques of compressional sound velocity parameter and wet-water, wet bulk density, and porosity parameter by gravimetric gamma ray attenuation techniques. In: Initial Reports. DSDP: 33, edited by Schlanger, S.O., Jackson, E.D. et al., Washington, D.C: U.S. Govt. Printing Office, 931–958.

Brudy, M. and M.D. Zobak (1998). Drilling-induced tensile wall-fractures: implications for determination of in-situ stress orientation and magnitude. International Journal of Rock Mechanics and Mining Sciences 36, 191–215.

Chang, C.D., L.C. McNeill, J.C. Moore, W. Lin, M. Conin and Y. Yamada (2010). In situ stress state in the Nankai accretionary wedge estimated from borehole wall failures. Geochemistry, Geophysics, Geosystems 11, 1–17.

Demets, C. R.G. Gordon, D.F. Argus and S. Stein (1990). Current plate motions. Geophysical Journal International 101, 425–478.

Ellis, D.V. (1986). Neutron porosity devices—what do they measure? First Break 4(3), 11–17.

Folk, R.L. (1968). Petrology of sedimentary rocks. Hamphill's Austin, Texas.

Folk, R.L. and W.C. Ward (1957). Brazos River. A study ion significance of grain–size parameters. Journal of Sedimentary Petrology 25, 3–27.

Gettemy, G.L. and H.J. Tobin (2003). Tectonic signatures in centimeter-scale velocity-porosity relationships of Costa Rica convergent margin sediments. Journal of Geophysical Research 108, B10, 2494.

Gough, D.I. and J.S. Bell (1982). Stress orientations from borehole wall fractures with examples from Colorado, east Texas, and northern Canada. Journal of Earth Science 19, 1358–1370.

Hamilton, E.L. (1970). Sound velocity and related properties of marine sediments, North Pacific. Journal of Acoustical Society of America 75, 4423–4446.

Hamilton, E.L. (1980). Geoacoustic modeling of the seafloor. Journal of Acoustical Society of America 68, 1313–1340.

Hamilton, E.L. and R.T. Bachman (1982). Sound velocity and related properties of marine sediments. Journal of Acoustical Society of America 72, 1891–1904.

Harris, R.N. G. Spinelli, C.R. Ranero, I. Grevemeyer, H. Villinger and U. Barckhausen (2010). Thermal regime of the Costa Rican Convergent margin: 2. Thermal models of the shallow Middle America subduction zone offshore Costa Rica. Geochemistry, Geophysics, Geosystems 11, 1–22.

Hey, R.N. (1977). Tectonic evolution of the Cocos, Nazca spreading center. Geological Society of America Bulletin 88, 1404–1420.

Husen, S. and E. Kissling (2001). Postseismic fluid flow after the large subduction earthquake of Antofagasta, Chile. Geology 29, 847–850.

Kimura, G. E. Silver and P. Blum (1997). Proceedings of the Ocean Drilling Program, Initial Reports, Volume 170, College Station, Texas (Ocean Drilling Program), 7–247.

Malinverno, A. S. Saito and P. Vannucchi (2016). Horizontal principal stress orientation in the Costa Rica Seismogenesis Project (CRISP) transect from borehole breakouts. Geochemistry, Geophysics, Geosystems 17, 65-77.

Moore, J.C. and D. Saffer (2001). Updip limit of the seismogenic zone beneath the accretionary prism of southwest Japan: An effect of diagenetic to low grade metamorphic processes and increasing effective stress. Geology 29, 183–186.

Moore, J.C. and P. Vrolijk (1992). Fluids in accretionary prisms. Review of Geophysics 30, 113–135.

Moore, J.C. G.J. Iturrino, P.B. Flemings and D.E. Sawyer (2009). Data report: Stress orientation from borehole breakouts. IODP Expedition 308. Ursa area, Mississippi Fan, Gulf of Mexico. In: Proceedings of the Integrated Ocean Drilling Program Expedition 308, edited by Flemings, P.B. et al., College Station, Texas, Integrated Ocean Drilling Program Management International, Inc.

Ranero, C.R. J.P. Morgan, K. McIntosh and C. Reichert (2003). Bending-related faulting and mantle serpentinization in the Middle America Trench. Nature 425, 367–373.

Ranero, C.R. A. Villaenor, J.P. Morgan and W. Weinrebe (2005). Relationship between bend-faulting at trenches and intermediate-depth seismicity. Geochemistry/Geophysics/Geosystems 6, 1-25.

Saito, S. A. Malinverno, Y. Yamamoto, W. Lin, Y. Kitamura, Y. Hashimoto, H. Wu, K. Ujiie, P. Vannucchi, N. Stroncik and IODP Expedition 334 Scientists (2011). Present-day principal horizontal stress orientations in the Costa Rica subduction zone: Preliminary estimates from logging-while-drilling, IODP Expedition 334, AGU Fall Meeting (Abstract), #T14B–05.

Stavenhagen, A.U. E.R. Flueh, C. Ranero, K.D. McIntosh, T. Shipley, G. Leandro, A. Shulze and J.J. Danobeitia (1998). Seismic wide-angle investigations in Costa Rica: a crustal velocity model from the Pacific to the Caribbean coast. Zb. Geol. Paläontol. 1997(3–6), 393–408.

Tobin, H. M. Kinoshita, K.T. Moe and the Expedition 314 Scientists (2009). Expedition 314 Summary. In: Proceedings of IODP. 314/315/316, edited by Kinoshita, M., Tobin, H., Ashi, J., Kumura, G., Lallemant, S., Screation, E.J., Curewitz, D., Masago, H., Moe, K.T., and the Expedition 314/315/316 Scientists (Eds.), Washington, D.C.

Trautwein-Bruns, U. K.C. Schulze, S. Becker, P.A. Kukla and J.L. Urai (2010). In situ stress variations at the Varican deformation front-Results from the deep Aachen geothermal well. Tectonophysics 493, 196–211.

Vannucchi, P. K. Ujiie, S. Stroncik, A. Malinverno and the IODP Exp. 334 Scientists (2012). Proceedings of the Integrated Ocean Drilling Program, Volume 334: Tokyo, IODP-MI.

Vannucchi, P. K. Ujiie, N. Stroncik and the IODP Exp. 334 Scientific Party (2013). IODP Expedition 334: An investigation of the sedimentary record, fluid flow and state of stress on top of the seismogenic zone of an erosive subduction margin. Scientific Drilling 15, 23–30.

Vannucchi, P. P.B. Sak, J.P. Morgan, K. Ohkushi, K. Ujiie and the IODP Expedition 334 Shipboard Scientists (2013). Rapid pulses of uplift, subsidence, and subduction erosion offshore Central America: Implications for building the rock record of convergent margins. Geology 41, 995–998.

von Huene, R. and D.W. Scholl (1991). Observations at convergent margins concerning sediment subduction, subduction erosion, and the growth of continental crust. Review of Geophysics 29, 279–316.
Walther, C.H.E. (2003). The crustal structure of the Cocos ridge off Costa Rica. Journal of Geophysical Research 108, 21–36.
Zobak, M.D. (2007). Reservoir geomechanics: Earth stress and rock mechanics applied to exploration, production and wellbore stability. Cambridge, Cambridge University Press, 449p.